Physical Communication 3 (2010) 1–18

Contents lists available at ScienceDirect

Physical Communication

journal homepage: www.elsevier.com/locate/phycom

Full length article

Emerging applications of wavelets: A review

Ali N. Akansu [a,*], Wouter A. Serdijn [c], Ivan W. Selesnick [b]

[a] New Jersey Institute of Technology, Department of Electrical & Computer Engineering, University Heights, Newark, NJ 07102, United States
[b] Polytechnic Institute of New York University, Department of Electrical & Computer Engineering, Six MetroTech Center, Brooklyn, NY 11201, United States
[c] Delft University of Technology, Faculty of Electrical Engineering, M & CS, Electronics Research Laboratory, Mekelweg 4, 2628 CD Delft, The Netherlands

ARTICLE INFO

Keywords:
Analog signal processing
Wavelet
Discrete wavelet
Discrete wavelet approximation
Analog wavelet filters
Subband transform
Filter bank
Iterative-thresholding

ABSTRACT

Although most of its popular applications have been in discrete-time signal processing for over two decades, wavelet transform theory offers a methodology to generate continuous-time compact support orthogonal filter banks through the design of discrete-time finite length filter banks with multiple time and frequency resolutions. In this paper, we first highlight inherently built-in approximation errors of discrete-time signal processing techniques employing wavelet transform framework. Then, we present an overview of emerging analog signal processing applications of wavelet transform along with its still active research topics in more matured discrete-time processing applications. It is shown that analog wavelet transform is successfully implemented in biomedical signal processing for design of low-power pacemakers and also in ultra-wideband (UWB) wireless communications. The engineering details of analog circuit implementation for these continuous-time wavelet transform applications are provided for further studies. We expect a flurry of new research and technology development activities in the coming years utilizing still promising and almost untapped analog wavelet transform and multiresolution signal representation techniques.

1. Historical perspective and current status

Multiresolution representation of image and video has always generated an interest in vision research due to the spectral properties and models of the human visual system (HVS). Burt and Adelson proposed their pyramid decomposition algorithm for multiresolution coding of image signals [1]. Their pioneering work opened the gate for a new image coding technique where better frequency localized subband transforms found their use as an alternative to the widely used discrete cosine transform (DCT) coding [2–4]. On the same track, Mallat looked into the continuous-time discrete wavelet transform as a multiresolution signal decomposition technique and its interconnections to discrete-time filter banks in his doctoral dissertation [5].

Independently, Daubechies elegantly formalized the theoretical linkage, first brought up by Mallat, between finite support orthonormal wavelet transform basis and two-band perfect reconstruction quadrature mirror filter (PR-QMF) bank in her seminal paper published in 1988 [6]. While Goupillaud, Grossmann, Morlet and other researchers in Europe made their early contributions, Daubechies' celebrated paper was the most significant starter for wavelet related research activities in the United States [7–9]. The New Jersey Institute of Technology Wavelets Symposium and the NSF CBMS Conference on Wavelets in 1990 [10,11] were the first two technical conferences in the Unites States where Signal Processing, Mathematics and other research communities shared the same venues for interdisciplinary exchanges and cross-fertilization have taken place.

Most of the relevant early work in signal processing field was to show and emphasize the theoretical interconnections and linkages between wavelet and subband transforms proven by Daubechies [6,12]. There were other

* Corresponding author.
E-mail addresses: akansu@njit.edu (A.N. Akansu), w.a.serdijn@tudelft.nl (W.A. Serdijn), selesi@poly.edu (I.W. Selesnick).

1874-4907/$ – see front matter © 2009 Elsevier B.V. All rights reserved.
doi:10.1016/j.phycom.2009.07.001

research contributions that offered filter bank solutions that lead to the design of compactly supported orthonormal wavelet bases. On the other hand, the theory of wavelet transforms were better understood by signal processing engineers and several tutorial papers on the subject published in the literature. A number of well written early research monographs, lecture notes and edited books on wavelet transforms and multiresolution signal processing and filter banks were published [13–15]. Then, there were many good quality papers and books on wavelet and subband transforms, and their applications published in the signal processing literature.

In addition to highlighting some novel implementation and applications of analog wavelet transforms, this review paper will describe wavelet transform approximation errors inherent in discrete-time signal processing and also some of the principle developments in wavelet theory for analog signal processing.

One of the important developments in the construction, design, and implementation of wavelet (multiscale) transforms is the design of geometrically-oriented two-dimensional (and higher) transforms. For example, starting with the steerable pyramid and continuing with the curvelet, contourlet, and shearlet, dual-tree complex wavelet transforms and wave atoms. These are especially important because some of the popular applications of multiscale transform are in image processing, for which these transforms make a substantial difference. In addition, these years have seen many advances in digital filter bank theory, for example in parameterizations, directional filter banks, and others. Additionally, the frequency domain design and FFT-based implementation of wavelet transforms has received new attention in the recent literature, for both one-dimensional and multidimensional non-separable geometrically-oriented transforms, because this approach overcomes limitations of FIR-filter-based designs. For example, using an FFT-implementation, orthonormal dyadic discrete wavelet transforms with symmetric filters and symmetric boundary extensions can be implemented for any signal length, including odd-lengths. In contrast, the conventional orthonormal FIR-convolution implementation cannot be simultaneously orthonormal and symmetric (excepting the Haar transform) and is furthermore usually implemented for signals whose lengths are powers of two.

One of the many active application areas of wavelet transform has been of denoising. The state-of the-art has progressed significantly over the last 20 years. For applications of denoising, the noise is rarely entirely Gaussian nor signal independent. Therefore, signal processing methods that can be applied to realistic scenarios are of continuing interest. Wavelet-based algorithms have also been developed for the problem of deconvolution. Some deconvolution and denoising algorithms can be unified into the framework of *iterative thresholding*. This approach has been proven to converge for certain problem formulations to a unique minimizer, and this theory serves as a foundation basis for further developments.

For many years the notion of sparsity been central in the motivation and effectiveness of wavelet transforms for compression, denoising, etc. Recently, important results regarding sparsity and L_1-norm minimization have been discovered and are fueling ongoing research activities. A recent issue of the *IEEE Signal Processing Magazine* is dedicated to Compressed Sensing [16], a sparsity-based approach to reduce the number of required measurements of signal.

Some of these discrete-time signal processing applications of wavelet transforms are further discussed in Section 4 of the paper.

As a multiresolution signal analysis technique, the wavelet transform offers the possibility of selective noise filtering and reliable parameter estimation, and therefore, can contribute efficiently to morphological analysis. For this reason wavelets have been extensively used in biomedical signal processing, mainly due to the versatility of the wavelet transform tools. Signal analysis methods derived from wavelet analysis carry large potential to support a wide range of biomedical signal processing applications including noise reduction, feature recognition and signal compression.

In implantable medical devices, such as pacemakers and implantable cardio defibrillators, power consumption is a critical issue due to the limited energy density and the longevity of currently available portable batteries. This implies that the design of such devices has to be optimized for very low-power dissipation. Due to the great relative power required for the analog-to-digital conversion and its marginal improvement in power efficiency over the years, it is predicted that the implementation of a fully digital wavelet signal processor in implantable pacemakers will not be feasible for several decades to come. For this reason, a method for implementing wavelet transform using continuous-time analog circuitry was proposed in Ref. [17], based on the development of ultra-low-power analog integrated circuits that implement the required signal processing, taking into account the limitations imposed by an implantable device.

The implementation of wavelet transform in an analog fashion is equivalent to the implementation of a filter whose impulse response is the desired (reversed) wavelet function. Hence, wavelet transform can be implemented by means of analog filters and filter banks. In implantable medical devices, minimization of the power consumption for a guaranteed performance reduces down to four important design steps as follows,

1. minimization of the total number of wavelet scales required, e.g., by introducing so-called multi-wavelets [18];
2. minimization of the order of the wavelet filter, i.e., finding a suitable approximation to the desired wavelet by means of a low-order rational transfer function [19];
3. optimization of the wavelet filter topology, i.e., finding the optimal state–space description implementing the wavelet filter transfer function [17,20]; and
4. optimizing the elementary wavelet filter building blocks, viz. the integrators.

Other applications that benefit from implementation of wavelet transform by means of analog circuitry are those that deal with high frequencies as required in portable and wearable wireless communication devices, as here the

restricted power consumption precludes the use of high-speed analog-to-digital and/or digital-to-analog converters. Examples of this kind can be found in ultra-wideband transmitters and in cognitive radio applications [21–23].

2. Discrete wavelet transform

2.1. Introduction

The wavelet transform maps the function $f(t)$ in $L^2(R)$ to another signal $W_f(a, b)$ in $L^2(R^2)$ where (a, b) are continuous, and called *scaling* and *shift* parameters, respectively. Although short time Fourier transform (STFT) decomposes a signal into a set of equal bandwidth basis functions in the spectrum the wavelet transform provides a decomposition based on constant-Q (equal bandwidth on a logarithmic scale) basis functions with improved multi-resolution characteristics in the time–frequency plane. Moreover, the wavelet parameters (a, b) are discretized in such a way that the orthogonality is still satisfied and the transform is performed on a grid within the continuous (a, b) plane.

We are going to present the fundamentals of wavelet transform, its continuous and discrete kinds for transforming continuous-time signals and implementation issues arise when we use them in digital signal processing applications.

2.2. Continuous wavelet transform of continuous-time (analog) signals

The mother wavelet or wavelet kernel $\psi(t)$ along with the continuous scaling and shift parameters (a, b) lead us to the definition of wavelet transform basis in the time and frequency domains as follows [6]

$$\psi_{ab}(t) = \frac{1}{\sqrt{a}}\psi\left(\frac{t-b}{a}\right) \leftrightarrow \Psi_{ab}(\Omega) = \sqrt{a}\Psi(a\Omega)\mathrm{e}^{-\mathrm{j}b\Omega}. \quad (1)$$

We can now define the continuous wavelet transform of continuous-time (analog) $f(t)$ as

$$W_f(a, b) = \langle f(t), \psi_{ab}(t)\rangle = \int_{-\infty}^{+\infty} f(t)\psi_{ab}(t)\mathrm{d}t \quad (2)$$

where the wavelet transform satisfies the invertibility conditions and the signal is recovered back from its wavelet coefficients as defined [6]

$$f(t) = \frac{1}{C_\psi}\int_{-\infty}^{+\infty}\int_{0}^{+\infty}\frac{\mathrm{d}a\mathrm{d}b}{a^2}W_f(a, b)\psi_{ab}(t) \quad (3)$$

with the requirement $C_\psi = \int_0^{+\infty}\frac{|\Psi(\Omega)|^2}{\Omega}\mathrm{d}\Omega < +\infty$ that implies zero-mean mother wavelet function as $\Psi(0) = \int_{-\infty}^{+\infty}\psi(t)\mathrm{d}t = 0$. Note that the mother wavelet is basically the impulse response of a continuous-time band-pass filter that decays at least as fast as $|t|^{1-\varepsilon}$ in time. Faster decay within this context implies better time localization of $f(t)$.

The continuous wavelet transform is not very practical and also quite redundant. Therefore, its continuous scaling and shift parameters (a, b) are discretized in discrete wavelet transform as defined in the next section.

2.3. Discrete wavelet transform of continuous-time (analog) signals

The continuous wavelet transform parameters (a, b) are sampled to reduce the redundancy and to make the wavelet transform more practical. Let us define the sampling grid $a = a_0^m$, $b = nb_0a_0^m$ and we can define the discrete wavelet transform basis as [6]

$$\{\psi_{mn}(t)\} = a_o^{\frac{-m}{2}}\psi(a_0^{-m}t - nb_0) \quad m, n \in Z. \quad (4)$$

If the set $\{\psi_{mn}(t)\}$ is complete for some $\psi(t)$, a, and b, then they are called *affine* wavelets. Therefore, we can express any $f(t) \in L^2(R)$ in the superposition of

$$f(t) = \sum_m\sum_n d_{m,n}\psi_{mn}(t) \quad (5)$$

where the discrete wavelet transform coefficients are defined as

$$d(m, n) = d_{m,n} = \langle f(t), \psi_{mn}(t)\rangle = \frac{1}{a_0^{m/2}}\int f(t)\psi(a_0^{-m}t - nb_0)\mathrm{d}t. \quad (6)$$

Such complete wavelet transform sets $\{\psi_{mn}(t)\}$ are called *frames*. Although they are complete they are not a basis yet since they do not satisfy the Parseval theorem. One can design a tight and exact frame leading to an orthonormal basis in $L^2(R)$ and satisfying

$$\int\psi_{mn}(t)\psi_{rs}(t)\mathrm{d}t = \begin{Bmatrix}1, & m = r, n = s\\ 0, & \text{otherwise}\end{Bmatrix}. \quad (7)$$

Note that these wavelet functions are orthonormal in both indices. Moreover, an orthonormal discrete wavelet transform is used to decompose a continuous-time signal into its wavelet basis functions.

Similarly, the complementary basis of discrete wavelet transform called scaling functions of multiresolution analysis also satisfy the following orthonormality condition within the same scale [6]

$$\int\phi_{mn}(t)\phi_{ms}(t)\mathrm{d}t = \delta_{n-s} \quad (8)$$

where for $a_0 = 2$ and $b_0 = 1$ we can define the scaling function set as

$$\{\phi_{mn}(t)\} = 2^{-m/2}\phi(2^{-m}t - n). \quad (9)$$

Moreover, we can obtain the scaling coefficients of $f(t)$ through the projection

$$c(m, n) = c_{m,n} = \langle f(t), \phi_{mn}(t)\rangle = \frac{1}{2^{m/2}}\int f(t)\phi(2^{-m}t - n)\mathrm{d}t. \quad (10)$$

The orthonormal wavelet and scaling bases jointly satisfy their complementary basis property as expressed

$$\int\psi_{mn}(t)\phi_{rs}(t)\mathrm{d}t = 0 \quad \text{for } \forall m, n, r, s. \quad (11)$$

It is noted that one must use infinitely many scales in the case of representing $f(t)$ in terms of discrete wavelet functions only as shown in Eq. (5). In contrast, we can

express $f(t)$ in a finite number of resolutions if we jointly utilize the scaling and wavelet basis functions as follows

$$f(t) = \sum_{n=\infty}^{+\infty} c_{L,n} 2^{-L/2} \phi\left(\frac{t}{2^L} - n\right) + \sum_{m=1}^{L} \sum_{n=-\infty}^{+\infty} d_{m,n} 2^{-m/2} \psi\left(\frac{t}{2^m} - n\right). \quad (12)$$

This expression is indeed a combination of a low-pass approximation to $f(t)$ utilizing the scaling function at *scale L* as expressed in the first term and the wavelet representation of the detail signal or approximation error given in the latter. This representation is clearly more efficient than the wavelet representation and also highlights the significant role of the scaling basis in the multiresolution signal decomposition framework based on wavelet transforms.

Note that the wavelet and scaling functions have the following inter-scale properties [6,14]

$$\psi(t) = 2 \sum_n h_1(n) \phi(2t - n)$$
$$\phi(t) = 2 \sum_n h_0(n) \phi(2t - n). \quad (13)$$

The coefficients $\{h_0(n)\}$ and $\{h_1(n)\}$ are called inter-scale basis coefficients. Their significance in the theory and design of wavelet transform is further explained in Section 2.4.

The mathematical highlights presented above require us to design a continuous-time mother wavelet $\psi(t)$ and its complementary scaling function $\phi(t)$ satisfying the intra-scale and inter-scale orthonormalities defined in Eqs. (7) and (8) in order to be able to achieve an orthonormal decomposition of a signal $f(t)$ into time and frequency localized bases functions in multiple and finite resolutions as shown in Eq. (12). We should emphasize that it would not be easy without Daubechies' multiresolution analysis framework that strongly links compactly supported orthonormal wavelet design problem with the relatively easier design of a discrete-time, two-band, finite length (FIR), perfect reconstruction quadrature mirror filter (PR-QMF) banks. Hence, the design of a compactly supported mother wavelet and its complementary scaling function in continuous time starts with designing a discrete-time two-band, FIR PR-QMF that will be explained in the following section.

2.4. Two-band FIR PR-QMF and compactly supported orthonormal wavelets

It can be shown that the continuous-time scaling function is obtained from the infinite resolution product of the discrete Fourier transform of the inter-scale coefficients $\{h_0(n)\}$ through the inverse Fourier transform defined as [6,14]

$$\Phi(\Omega) = \prod_{k=1}^{+\infty} H_0(e^{j\frac{\omega}{2^k}}) \leftrightarrow \phi(t) \quad 0 \le t \le (N-1)T_0$$
Assume $T_0 = 1$ (14)

where discrete-time Fourier transform (DTFT) of $\{h_0(n)\}$ is expressed in $H_0(e^{j\omega}) = \sum_{n=0}^{N-1} h_0(n) e^{-j\omega n}$. Similarly, the orthonormal wavelet function of compact support is also obtained from its inverse Fourier transform as shown in

$$\Psi(\Omega) = H_1\left(e^{j\frac{\omega}{2}}\right) \prod_{k=2}^{+\infty} H_0\left(e^{j\frac{\omega}{2^k}}\right)$$
$$\leftrightarrow \psi(t) \quad 1 - \frac{N}{2} \le t \le \left(\frac{N}{2}\right) T_0 \text{ Assume } T_0 = 1. \quad (15)$$

Note that the sequences $\{h_0(n)\}$ and $\{h_1(n)\}$ are defined in the time interval $0 \le n \le N-1$ and have the following relationship $H_1(e^{j\omega}) = e^{-j\omega(N-1)} H_0(-e^{-j\omega})$. Now, if we impose the orthonormality conditions of Eqs. (7) and (8) on the design of $\{\psi(t)\}$ and $\{\phi(t)\}$ it turns out that the inter-scale coefficient sequences $\{h_0(n)\}$ and $\{h_1(n)\}$ must satisfy the discrete-time domain conditions [6,14]

$$\sum_n h_r(n) h_s(n + 2k) = \begin{cases} \delta(k) & r = s \\ 0, & r \ne s \\ r, & s = 0, 1 \end{cases} \quad (16)$$
$$h_1(n) = (-1)^{n+1} h_0(N - 1 - n); \quad N \text{ is even.}$$

These conditions might also be reduced to the corresponding frequency domain properties imposed on $H_0(e^{j\omega})$ and $H_1(e^{j\omega})$as follows

$$|H_0(e^{j\omega})|^2 + |H_1(e^{j\omega})|^2 = 1$$
$$H_0(e^{j\omega})|_{\omega=\pi} = H_0(e^{j\omega})|_{\omega=0} = 0. \quad (17)$$

A careful examination of this result and previous discussions show us that if one wants to design compactly supported, orthonormal, discrete wavelet and scaling transform bases, he should first design a two-band PR-QMF bank satisfying Eq. (17) and $H_0(e^{j\pi}) = H_1(e^{j0}) = 0$, then plug them into Eqs. (14) and (15) yielding the desired continuous-time functions [12,14].

2.5. Discrete wavelet transform of discrete-time signals and approximation errors

Although the continuous and discrete wavelet transforms are both defined for the multiresolution mapping of continuous-time signals, most of their popular applications reported in the signal processing literature are in discrete-time signal processing. In contrast, we highlight analog implementations of wavelet transform for a few emerging analog signal processing applications in Section 3. Moreover, we also discuss and quantify the inherent approximation errors below in case one employs a discrete wavelet transform to process an already sampled discrete-time signal where its analog counterpart is not known to us.

2.5.1. Approximation error due to imperfect generation of wavelet and scaling bases

Theoretically, the generation of mother wavelet and its complementary scaling functions defined in Eqs. (15) and (14), respectively, requires infinitely many terms in the product operations in the frequency domain. In reality,

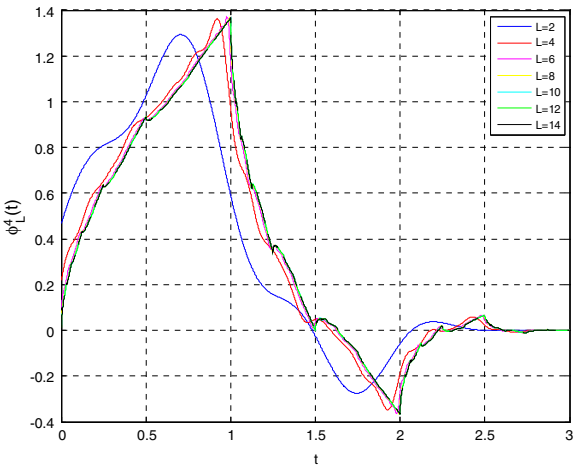

Fig. 1a. Approximations to the $\{\phi_L(t)\}$ scaling functions for 4-tap Daubechies wavelet filters with various values of L in Eq. (18).

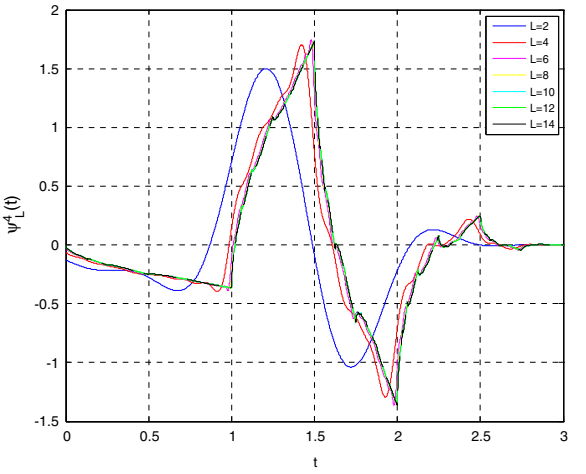

Fig. 1b. Approximations to the $\{\psi_L(t)\}$ wavelet functions for 4-tap Daubechies wavelet filters with various values of L in Eq. (19).

the order of these products is of finite as expressed below [6,14],

$$\Phi_L(\Omega) = \prod_{k=1}^{L} H_0(e^{j\frac{\omega}{2^k}}) \tag{18}$$

$$\Psi_L(\Omega) = H_1(e^{j\frac{\omega}{2}}) \prod_{k=2}^{L} H_0(e^{j\frac{\omega}{2^k}}). \tag{19}$$

Then, through the inverse Fourier transform we obtain the time domain approximations to the corresponding wavelet and scaling functions as $\phi_L(t) \leftrightarrow \Phi_L(\Omega)$ and $\psi_L(t) \leftrightarrow \Psi_L(\Omega)$.

The functions $\psi_L(t)$ and $\phi_L(t)$ are different than the theoretically defined wavelet and scaling functions $\psi(t)$ and $\phi(t)$. Indeed, it is impossible to obtain the latter since it requires infinitely many terms in the product. Figs. 1a and 1b displays approximations to the scaling and wavelet functions generated by using 4-tap Daubechies PR-QMF with various values of L in Eqs. (18) and (19), respectively.

We would like to quantify the approximation errors of scaling and wavelet functions due to finite number of terms used in their generation. Let us define mean square error (mse) of approximations for wavelet and scaling functions as follows

$$e_\phi^N(L) = \int [\phi_\infty^N(t) - \phi_L^N(t)]^2 dt \tag{20a}$$

$$e_\psi^N(L) = \int [\psi_\infty^N(t) - \psi_L^N(t)]^2 dt \tag{20b}$$

where N is the number of filter taps in a two-band PR-QMF bank. Fig. 2 displays $e_\phi^N(L)$ and $e_\psi^N(L)$ for Daubechies wavelets family for $N = 4$. We assumed that $\phi_\infty^N(t) = \phi_{14}^N(t)$ and $\psi_\infty^N(t) = \psi_{14}^N(t)$ in Eqs. (14) and (15) due to the limitations of computational power we had and then, we calculated mse of Eq. (20) for various cases and displayed them in Fig. 2.

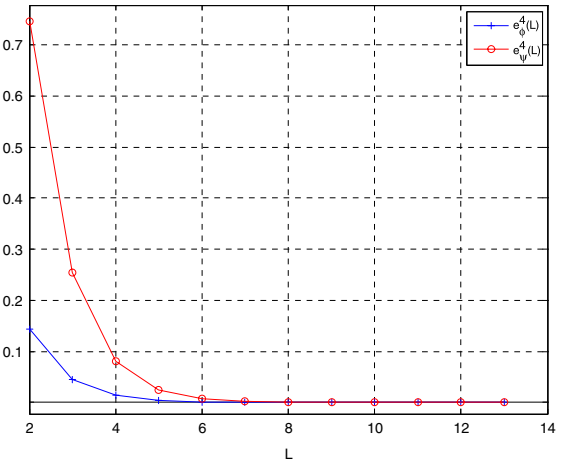

Fig. 2. Mean square errors (mse) of various approximations to Daubechies wavelet and scaling functions for $N = 4$ defined in Eqs. (20a) and (20b).

2.5.2. Wavelet approximation error due to sampling of signals

In order to highlight and visualize the following theoretical discussions we define an arbitrary continuous-time signal $f(t)$ expressed as,

$$f(t) = \cos(2\pi 0.5t) + 0.5\sin(2\pi 0.2t) + 3\sin(2\pi 0.1t) + 2\cos(2\pi 0.3t) - 2\cos(2\pi 0.4t).$$

Then, we sample $f(t)$ as $f(n) = f(nT_s) = f(t)|_{t=nT_s} T_s = 1\,\text{s}$. $f_s = \frac{1}{T_s} = 1\,\text{Hz}$.

On the other hand, let us calculate the scaling coefficients $\{c_{m,n}\}$ of $f(t)$ for scale $m = 0$ as defined in Eq. (10)

$$c(n) = c_{0,n} = \langle f(t), \phi_{0,n}(t)\rangle = \int f(t)\phi(t-n)dt.$$

Since $c(n) \neq f(n)$, we now define the error signal and normalized mean square error between $f(n)$ and $c(n)$ sequences as follows,

$$e(n) = f(n) - c(n) \tag{21a}$$

$$e_{mse} = \frac{1}{K}\sum_{n=0}^{K-1}\frac{[e(n)]^2}{[f(n)]^2}. \quad (21b)$$

Fast wavelet transform

Note that two-band orthonormal PR-QMF based discrete-time dyadic (octave band or constant-Q) filter bank offers a fast wavelet transform implementation for continuous-time $f(t)$ function *iff* it is completely represented within the *scaling subspace* of the resolution $m = 0$ of multiresolution signal analysis framework as $f(t) \in L^2(R)$ and $f(t) \in V_0$; $d(n) = d_{0,n} = 0$, and if its discrete-time input sequence is basically the scaling coefficients of the scale $m = 0$ as described above, namely $f(n) = c(n)$ and $d(n) = 0$ [6,14]. Then, as an example, the subband signal samples of this dyadic filter bank for subbands like *H, LH, LLH, LLLH* are identical to the corresponding wavelet coefficients $d(1, n)$, $d(2, n)$, $d(3, n)$ and $d(4, n)$ of those resolution scales for $m = 1, 2, 3, 4$, respectively, where L stands for low frequency half-band, and H stands for high frequency half-band of a two-band PR-QMF [6,14].

These FIR PR-QMF filter sequences $\{h_0(n)\}$, $\{h_1(n)\}$ are also used to generate the corresponding scaling and wavelet functions of this multiresolution analysis as defined in Eqs. (18) and (19).

Similarly, the output samples of the discrete-time *LLLLL* subband is equal to the scaling coefficients of that resolution scale $m = 5$ represented as $c(5, n)$. In such a situation, the theoretical requirement of $f(n) = c(n)$ for a *fast wavelet transform* implementation in multiresolution analysis employing a discrete-time two-band PR-QMF based discrete-time dyadic filter bank perfectly holds *only* for Shannon *wavelets* that are generated by using the ideal low-pass and high-pass discrete-time filters of a two-band PR-QMF, $\{h_0(n)\}$, $\{h_1(n)\}$ as given in Eqs. (14) and (15), and also with the requirement of $d(n) = d_{0,n} = 0$. Therefore, all other wavelet decompositions performed on already sampled signals inherently have the wavelet transform approximation errors due to the theoretical facts that

(a) an arbitrary continuous-time signal $f(t) \in L^2(R)$ can be approximated by $P_{-1}f(t)$, its projection onto subspace V_{-1} expressed as $P_{-1}f(t) = P_0f(t) + Q_0f(t)$ with the orthogonal complement property $V_{-1} \in V_0 \oplus W_0$ and $V_0 \perp W_0$ where V_0 and W_0 are the scaling and wavelet subspaces, respectively, in the resolution level $m = 0$; therefore, $d(n) = d_{0,n} \neq 0$, and

(b) using the samples of $f(t)$ as the input sequence of the dyadic filter bank rather than calculating the scaling coefficients $c(n) = \{c_{0,n}\} =< f(t), \phi_{0,n}(t) >= \int f(t)\phi(t-n)\mathrm{d}t$ of that multiresolution analysis as required for the fast wavelet transform implementation discussed above. The readers of more theoretical interest are referred to the References [6,14] for detailed treatment of this point.

Fig. 3 displays $e(n)$ of Eq. (21) along with $\{f(n)\}$ and $\{c(n)\}$ sequences for the case of 4-taps Daubechies wavelet filter and $f(t)$ defined above. It is noted that e_{mse} is equal to 0.022 for this case. Fig. 4 displays e_{mse} versus L defined in Eq. (21) for both 4-taps and 8-taps cases. This important theoretical fact has been overlooked by many researchers in the literature employing wavelet

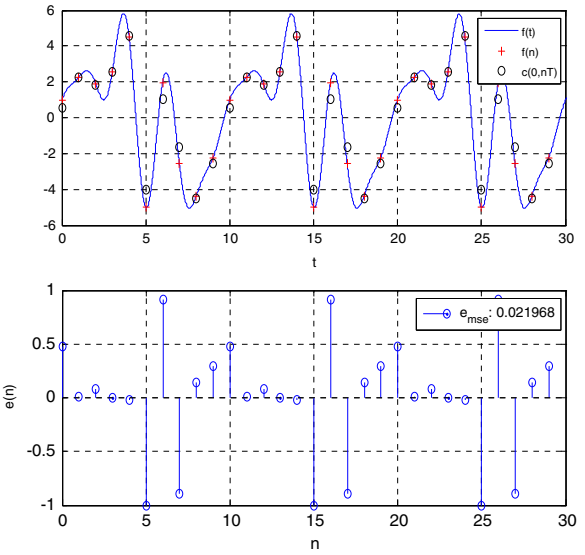

Fig. 3. $e(n)$ along with $f(n)$ and $c(n)$ for 4-taps Daubechies wavelet filters used in Eqs. (14) and (15) with $L = 14$. The resulting approximation error is $e_{mse} = 0.022$.

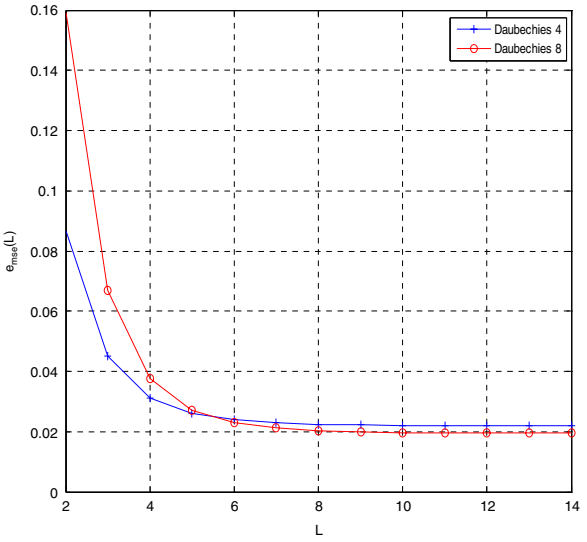

Fig. 4. Normalized mean square errors (mse) defined in Eq. (21b) calculated for various approximations to 4-length and 8-length Daubechies scaling functions.

decomposition for discrete-time (already sampled) signals using discrete-time filter banks. It is noted that discrete-time subband transform (filter bank) theory and methods offer an error-free and complete theoretical framework for multiresolution decomposition of discrete-time signals.

In the next two sections, we present several emerging analog applications of wavelet transform emphasizing its almost untapped and tremendous potential as a continuous-time signal processing framework in future research and technology development along with a few more commonly known discrete-time applications.

3. Analog signal processing applications of discrete wavelet transform

In Section 2, it was already mentioned that the mother wavelet function basically is the (reversed) impulse response of a continuous- or discrete-time band-pass filter. As a consequence, the discrete wavelet transform may thus be implemented by an analog filter bank, comprising of continuous- or discrete-time wavelet filters where each implements one (e.g., dyadic) scale of the multiresolution wavelet transform.

The starting point of the wavelet filter design trajectory presented here is the definition of its transfer function or, equivalently, a differential equation, describing its input–output relation. However, a linear differential equation having a predefined desired impulse response does not always exist. Hence, one needs to use a suitable approximation method covered in Section 3.1. There are several mathematical techniques that are frequently used to achieve the best approximation possible. Nonetheless, one of the most important aspects of analog wavelet filter synthesis is that the approximating function must lead to a physically realizable network which is dynamically stable.

Next, as there are many possible state–space descriptions and thus filter topologies that implement a particular transfer function, the designer has to find one that fits specific design requirements. Since in many applications like in wearable or implantable medical devices, the power consumption must be minimized to ensure long operation times from a battery, we optimize the state–space description of the wavelet filter for dynamic range, insensitivity to component variations and sparsity as discussed in Section 3.2. We will focus on a synthesis technique that is exclusively based on (continuous- or discrete-time) integrators. In order to implement a discrete-time wavelet filter, one must obtain a transfer function in the Z-domain. In contrast, a continuous-time wavelet filter is described mathematically by a rational function in the Laplace domain.

The last step deals with the design of the integrator that is the main building block of a wavelet filter. It is discussed in Section 3.3 in detail.

Finally in Section 3.4, we discuss two applications of analog wavelet filters, namely circuits for the real-time analysis of EKG (electrogram) signals and pulse generators for ultra-wideband communications.

3.1. Finding a suitable approximation to desired wavelet by a low-order rational transfer function

The available methods for generating the filter transfer function can be classified as the *closed-form* and the *iterative* techniques. In closed-form methods, the transfer function is derived from a set of closed-form formulas or transformations. Some classical closed-form solutions are the so-called Butterworth, Chebyshev, Bessel-Thompson and elliptic approximations. Iterative methods entail a considerable amount of computation and they can be used to design filters with arbitrary responses.

If the desired wavelet filter transfer function does not have an explicit expression, then the splines based interpolation method can be used to generate the desired (idealized) function that can be used as a starting point for the filter design process.

In electronic filters, the power consumption and the dynamic range are proportional and inversely proportional to the order of the filter, respectively. In this design step, the joint optimization of power consumption and dynamic range means finding a low-order rational approximation to the Laplace transform of the desired wavelet filter transfer function. In the sequel, we will deal with two techniques in order to achieve such an approximation. They are (a) the *Padé approximation* and (b) the L_2 *approximation* as described below.

(a) The Padé Approximation: It is employed to approximate the Laplace transform of the desired filter transfer function $G(s)$ by a suitable rational function $H(s)$ [24]. It is characterized by the property that the coefficients of the Taylor series expansion of $H(s)$ around a selected point $s = s_0$ coincide with the corresponding Taylor series coefficients of $G(s)$ up to the highest possible order, given the pre-specified degrees of the numerator and denominator polynomials of $H(s)$. If we denote the Padé approximation $H(s)$ of order (m, n), with $m \leq n$, at $s = s_0$, by

$$H(s) = \frac{p_0(s - s_0)^m + p_1(s - s_0)^{m-1} + \cdots + p_m}{(s - s_0)^n + q_1(s - s_0)^{n-1} + \cdots + q_n} \tag{22}$$

then there are $m + n + 1$ degrees of freedom. This generically makes it possible to match exactly the first $m + n + 1$ coefficients of the Taylor series expansion of $G(s)$ around $s = s_0$. This matching problem can easily be rewritten as a system of $m + n + 1$ linear equations in the $m + n + 1$ variables $p_0, p_1, \ldots, p_m, q_1, \ldots, q_n$, and a unique solution is obtained easily. Moreover, a good match is guaranteed between the given function $G(s)$ and its approximation $H(s)$ in a neighborhood of the selected point s_0.

However, there are also some disadvantages limiting the practical applicability of this technique [25]. One important issue concerns the selection of the point s_0. Note that a good approximation of $G(s)$ around one point in the (complex) Laplace domain is not a requirement per se. The second important issue is the stability. It does not automatically result from the Padé approximation technique. For example, if emphasis is put on obtaining a good fit for a particular s_0, it may easily happen that the resulting approximation becomes unstable. The trade-off between a good fit near a certain point $s = s_0$ and stability is a non-trivial problem. The third design issue is the choice of the degrees m and n for the numerator and denominator polynomials of the rational approximation $H(s)$. An improper choice may yield an inconsistent system of equations yielding an unstable approximation.

(b) L_2 Approximation: It is an alternative to the Padé approximation offering a number of advantages [19,25]. First of all, on the conceptual level, it is quite appropriate to use the L_2-norm to measure the quality of an approximation $H(s)$ to the function $G(s)$. Another advantage of L_2 approximation is that it can be applied both in the time domain as well as in the Laplace domain.

According to the Parseval theorem, minimization of the squared L_2-norm of the difference between $G(s)$ and $H(s)$ over the imaginary axis $s = j\omega$ in the complex plane is equivalent to minimization of the squared L_2-norm of the difference between $g(t)$ and $h(t)$ functions in the time domain. Particularly in the case of low-order approximation, the L_2 approximation can be achieved in a simple and straightforward way using standard numerical optimization techniques and software tools available.

3.2. Finding state–space description of optimal wavelet filter

After we complete the design of the wavelet filter transfer function, we design the wavelet filter topology. Since there are many possible state–space descriptions for a particular transfer function, many possible filter topologies exist. We will concentrate on finding a filter topology that is optimized for both dynamic range and power consumption.

It is well known from linear systems theory that any causal and linear filter of finite order n can be represented in the Laplace domain as a state–space system ($\mathbf{A}$, $\mathbf{B}$, $\mathbf{C}$, $\mathbf{D}$), described in a set of associated polynomial equations of the form,

$$\begin{aligned} s\mathbf{X}(s) &= \mathbf{A}\mathbf{X}(s) + \mathbf{B}U(s) \\ Y(s) &= \mathbf{C}\mathbf{X}(s) + \mathbf{D}U(s) \end{aligned} \tag{23}$$

where $U(s)$ denotes the scalar input to the filter, $Y(s)$ is the scalar filter output and $\mathbf{X}(s)$ is the state vector.

The transfer function of the filter is given by

$$H(s) = \mathbf{C}(s\mathbf{I} - \mathbf{A})^{-1}\mathbf{B} + D. \tag{24}$$

For the discrete-time case, similar expressions hold in the Z-domain.

The dynamic range of a system is essentially determined by the maximum processable signal magnitude and the internally generated noise. It is well known that the system's controllability and observability gramians play a key role in the determination and optimization of the dynamic range [26,27]. The controllability ($\mathbf{K}$) and observability ($\mathbf{W}$) gramians are derived from the state–space description and they are computed by solving the equivalent Lyapunov equations

$$\mathbf{A}\mathbf{K} + \mathbf{K}\mathbf{A}^{\mathrm{T}} + 2\pi\mathbf{B}\mathbf{B}^{\mathrm{T}} = 0 \tag{25}$$

and

$$\mathbf{A}^{\mathrm{T}}\mathbf{W} + \mathbf{W}\mathbf{A} + 2\pi\mathbf{C}^{\mathrm{T}}\mathbf{C} = 0. \tag{26}$$

Since the dynamic range of a circuit is defined as the ratio of the maximum and the minimum signal levels it can process, optimization of the dynamic range is equivalent to the simultaneous maximization of the (distortionless) output swing and the minimization of the overall noise contribution. In Ref. [28], Rocha gives a geometric interpretation for the optimization of the dynamic range. A visualization of the optimization procedure is displayed in Fig. 5 for a system with three state variables. The output swing is related, via the controllability gramian, to the space of "occurring" state–space vectors. Under the assumption of a random input signal, the shape of this space is generally a multidimensional ellipsoid. The constraint that each integrator has a maximum representation capacity M defines a multidimensional cuboid that, for a distortionless transfer function, should contain the former mentioned ellipsoid completely. As the mean square radius of the ellipsoid is equivalent to the maximum output swing, the output swing is maximized when the mean square radius is maximal. This can occur if and only if the ellipsoid becomes a spheroid. In that case the controllability gramian is a diagonal matrix with equal diagonal entries. It means that all axes of the ellipsoid have equal lengths. Therefore, the first optimization step boils down to a similarity transform such that the controllability gramian of the new system becomes a diagonal matrix with equal diagonal entries.

In the second step of the optimization procedure, the system is optimized with respect to its noise contribution. Rocha defines another ellipsoid representing the noise that is added to the state vector in each direction. While preserving the result of the first optimization step, it is possible to rotate the state–space such that the observability gramian becomes a diagonal matrix as well. In that case, the axes of the noise ellipsoid are aligned with the "system axes".

In order to maximize the dynamic range of the system, it is shown in Ref. [28] that one should minimize the objective function representing the relative improvement of the dynamic range and contains all parameters that are subject to manipulation by the designer. This objective function is expressed as

$$F_{DR} = \frac{\max_i k_{ii}}{(2\pi)^2} \sum_i \frac{\alpha_i}{C_i} w_{ii} \tag{27}$$

where k_{ii} and w_{ii} are the main diagonal elements of $\mathbf{K}$ and $\mathbf{W}$, respectively, $\alpha_i = \sum_i A_{ii}$ is the absolute sum of the elements on the ith row of $\mathbf{A}$, and C_i is the capacitance in integrator i.

Finally, exploiting the well known fact that the relative noise contribution of an integrator decreases when the capacitance and bias current increase, we apply noise scaling, i.e., we match an optimal capacitance distribution to the noise contributions of each individual integrator, viz. the diagonal entries of $\mathbf{W}$, combined with the coefficients in matrix $\mathbf{A}$ resulting in [28]

$$C_i = \frac{\sqrt{\alpha_i w_{ii} k_{ii}}}{\sum_i \sqrt{\alpha_i w_{ii} k_{ii}}} \cdot C_{\mathrm{tot}}. \tag{28}$$

C_{tot} being the total capacitance of the wavelet filter. The drawback of a dynamic-range optimal system is that its state–space matrices are generally fully dense, i.e., all the entries of $\mathbf{A}$, $\mathbf{B}$, $\mathbf{C}$ are filled with nonzero elements. These coefficients will have to be mapped on circuit components and it will result in a complex circuit with a large number of interconnections. For high-order filters it is therefore necessary to investigate how a realization of the desired transfer function having sparser state–space matrices would compare to the one having maximal dynamic range. Also, when designing high-order filters, it is very desirable to concentrate on circuits that are less sensitive to component variations. It is known that

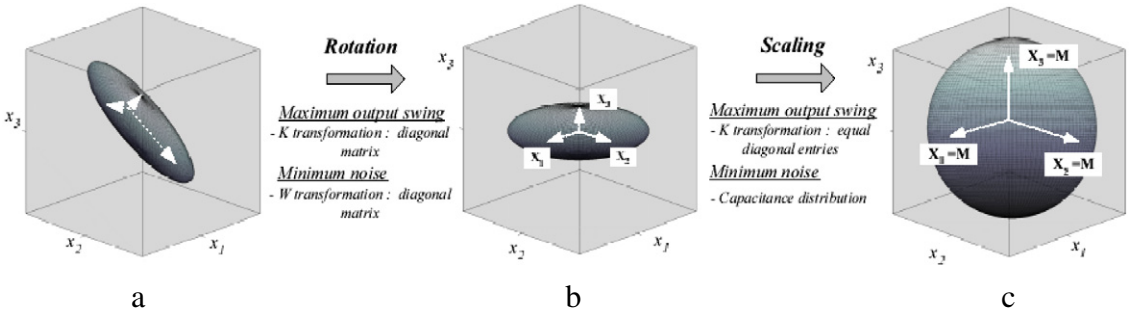

Fig. 5. Dynamic-range optimization based on the similarity transformation of **K**, **W** and capacitance distribution. The coordinate axes represent the state variables and the cuboid represents the maximum signal amplitude (**M**) that the integrators are able to handle. (a) The initial state–space representation (ellipsoid) is usually not well adapted to the integrators' representation capacity bounds (cuboid). (b) The (rotated) ellipsoid's principal axes are now aligned to the coordinate axes as a result of the diagonalization procedure to the matrices **K** and **W**. (c) Finally, the optimized state representation is obtained by scaling the state variables and the noise. Note that the sphere represents the maximum possible mean square radius which can be fitted into the integrators' capacity cuboid.

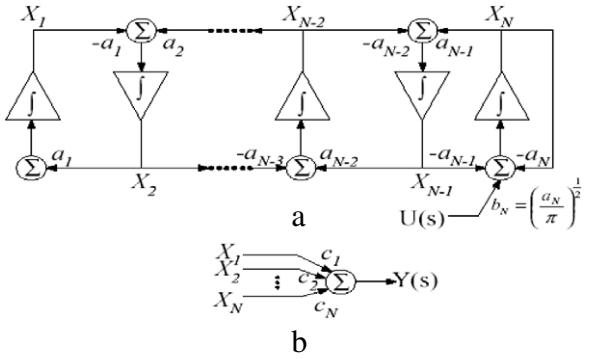

Fig. 6. Block diagram of an orthonormal ladder filter [20], (a) Leapfrog structure, (b) Output summing stage.

an optimal dynamic-range system will also have optimal, i.e., minimal, sensitivity [29]. For a less complex circuit, it is possible, for instance, to reduce **A** to upper triangular by a Schur decomposition, and therefore, reducing the number of nonzero coefficients in **A**. However, this transformation leads to an increase in the system noise and consequently to an increase in the objective function F_{DR} in Eq. (27). Another possibility is the *orthonormal ladder structure* [20] that is significantly sparser than the fully dense **A** matrix of the dynamic-range optimized system and the Schur decomposition. And, it still presents a good behavior with respect to sensitivity.

Fig. 6 shows a block diagram of a general orthonormal ladder filter [20]. The filter output is obtained from a linear combination of the outputs of all integrators.

The **A** matrix of an orthonormal ladder filter is tri-diagonal and is very nearly skew-symmetric except for a single nonzero diagonal element. The **B** vector consists of all zeros except its *n*th element. Another property of orthonormal ladder filters is the fact that the resulting circuits are inherently state scaled, i.e., the controllability gramian is already an identity matrix. The drawback of this structure is that the system is not optimized with respect to its noise contribution. However, if an optimal capacitance distribution is applied to this suboptimal system, it can still yield some extra gain compared to the case of equal capacitances. Often this leads to a filter topology that is not too complex and it has a dynamic range that is close (i.e., within a few dBs) to the optimal solution.

3.3. Wavelet filter integrator design

After an optimal wavelet filter topology is selected and the appropriate coefficients are chosen, we design the main building block of the wavelet filter circuit, viz. the integrator, as follows.

3.3.1. Four integrator classes

In order to be able to construct the wavelet filter topology, the transfer function of the integrators should be dimensionless. In an integrated circuit, i.e., on a chip, the integrating element is a capacitor, which can be employed as a (passive) capacitance or as part of an active trans-capacitance (amplifier) and whose transfer function has a dimension Ω. To realize a dimensionless integrator transfer function, we thus need an additional (trans)conductance (with a dimension Ω^{-1}). Hence, the following four types of integrators can be distinguished for our purposes. Namely,

(a) conductance–capacitance integrators,
(b) conductance–transcapacitance integrators,
(c) transconductance–capacitance (gm–C) integrators, and
(d) transconductance–transcapacitance integrators.

Fig. 7 depicts the four integrator types that implement a voltage-to-voltage integration.

The *conductance–capacitance* integrator does not use active components. Both the required conductance and integration are implemented passively without the use of transistors. As a result, using this type of integrator, it is not possible to implement filter transfer functions with complex poles.

The second type of integrator, the *conductance–transcapacitance* integrator, does not have this drawback. Thus, it is used more often. In this type of integrator, the realization of the actual integration function is an active transcapacitance often comprising an operational amplifier (op amp) having a capacitor in its (shunt) feedback path. The opamp

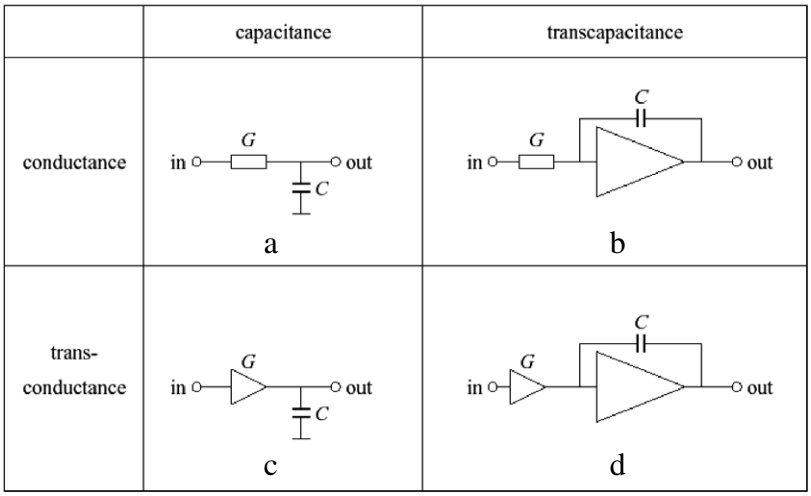

Fig. 7. Four integrator classes.

can be designed to operate rail-to-rail at the output terminals. Therefore, a full advantage of the supply voltage is utilized leading to an optimal dynamic range. The conductance can be integrated as a resistor. It could also be implemented as a MOS transistor in the triode region thus yielding a *MOSFET-C integrator* [30].

The third integrator type, the *transconductance–capacitance* integrator, makes use of active conductances, i.e., transconductances. The advantage of transconductors is that they are able to operate at relatively high frequencies due to the fact that their parasitic capacitances at the input and output nodes are in parallel with the integrator capacitors. Thus, they can easily be accounted for in the dimensioning of the required capacitor [31]. A major drawback, however, is that it is very difficult to implement transconductors with rail-to-rail input capability and thus with maximum dynamic range.

The fourth type is the *transconductance–transcapacitance* integrator. This integrator has no advantages over the second and third integrators mentioned. Its important disadvantage is the use of two active parts, both adding to the distortion, the power consumption and the noise production.

In conclusion, the second and third types of integrators are preferred when one designs wavelet filters. An active part is required for both of these integrator types.

3.3.2. ELIL and ELIN

As integrators consist of two parts, a (trans)conductance and a (trans)capacitance, based on the relationships of the intermediate quantity to the input and/or output quantity, linear integrators, our main wavelet filter building blocks can be further classified into two categories [32]. Namely,

(a) externally linear, internally linear (ELIL), and
(b) externally linear, internally non-linear (ELIN).

Most of the known integrator types fall into the first category, ELIL. In ELIL integrators, the intermediate quantity is linearly related to the input and output quantities. Among them are the integrator topologies that are commonly referred to as *Gm-C*, *MOSFET-C*, *opamp-RC*, *RC* and even (albeit discrete time rather than continuous time) *switched-capacitor (SC)* integrators.

In ultra-low-power (i.e., nano- and micro-power) applications, resistors would become too large for integration on chip, occupying a large chip area, having a small bandwidth or suffering from large absolute tolerances. For these cases, we will resort to ELIN integrators.

For the second category, ELIN integrators, it holds that their external behavior is precisely linear, yet the intermediate quantity is non-linearly related to its input and output quantities. Here, we find the subcategory of instantaneously companding[1] integrators, i.e., the degree of compression/expansion at a given instant depends only on the value of signals at that instant [32,33]. Belonging to this subcategory, the class of *dynamic translinear* [33] (also known as *log-domain* [34–36] or *exponential state–space* [37]) is probably the most well known. To the subcategory of companding integrators, albeit discrete time rather than continuous time, also belong *switched current* [38] and *switched MOSFET* [39,40] integrators. We will give an example of a dynamic translinear wavelet filter for biomedical applications in the next subsection.

3.4. Applications of analog wavelet filters

3.4.1. Low-power implementation of analog wavelet filter bank for biomedical signal processing and pacemakers

The detection of action potentials is an important function in many wearable and implantable medical devices. A well known example is the so-called "sense amplifier" in cardiac pacemakers designed to detect the QRS complex in the cardiac cycle in real time. Over the years, many systems have been devised in order to perform this task. They all have in common that they comprise of a filtering stage (performing linear and/or non-linear filtering) and a decision stage (comprising of peak detection and decision

[1] Companding is a combination of compressing and expanding.

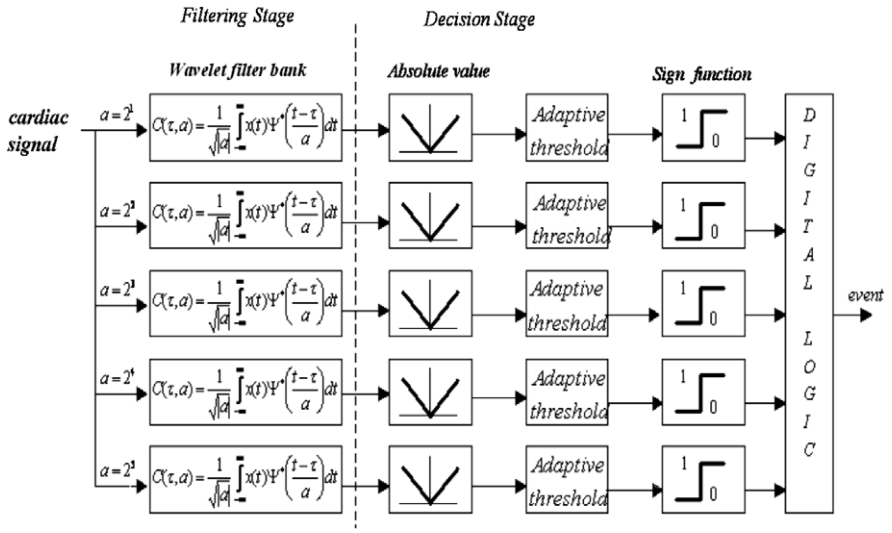

Fig. 8. Wavelet-based QRS modulus maxima detection system [41].

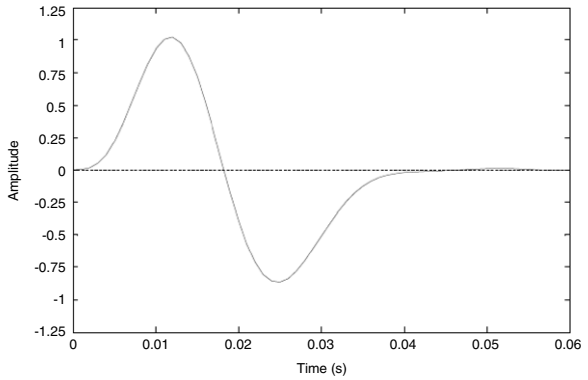

Fig. 9. Sixth-order L_2 approximation of *gaus*1 wavelet function.

logic). The detection of the QRS complex presented here is based on the detection of the modulus maxima of the wavelet transform.

The proposed block diagram is displayed in Fig. 8 [41].

At the input, wavelet filters are situated to implement an approximation to the first derivative Gaussian wavelet transform. The complete filter bank comprises of a bank of wavelet filters in order to compute the various scales of the wavelet transform in real time. Subsequently, the signal is fed through an absolute value circuit, followed by a peak detector and an adaptive threshold detector detecting the peak level of the rectified wavelet filter signal.

For the approximation to the *gaus*1 wavelet base, a sixth-order L_2 approximation is used. The resulting wavelet filter transfer function is expressed as

$$H_{[4/6]}(s) = \frac{-0.16s^4 + 8.32s^3 - 6.64s^2 + 139s}{s^6 + 5.9s^5 + 30.5s^4 + 83.1s^3 + 163s^2 + 176s + 93.3} \quad (29)$$

and its corresponding impulse response is shown in Fig. 9.

For the wavelet filter topology, an orthonormal ladder filter is defined as discussed above. The block diagram of the sixth-order orthonormal wavelet filter employing transconductance–capacitor integrators is displayed in Fig. 10.

In an ultra-low-power application such as cardiac pacemakers, it is often more convenient to implement the integrators in an ELIN fashion as discussed above. For this example, we have adopted the dynamic translinear circuit technique to implement the integrators in the orthonormal wavelet filter and also to implement the subsequent rectifier, peak detector and comparator. The circuit details of this design example can be found in Ref. [41].

In order to verify the performance and efficacy of the wavelet-based QRS modulus maxima detection system, a set of cardiac signals was applied to the input of the system. Fig. 11a shows the ideal wavelet transform for 5 scales with a ventricular IECG signal at the input. Fig. 11b gives the circuit simulation result of a sixth-order wavelet filter bank. On the left, we see the cardiac signal and 5 scales of the discrete wavelet transform. On the right, the modulus maxima (the white regions) are depicted also for 5 scales. One clearly can see the similarity between the ideal wavelet transform and the performance of the implemented system.

The circuit was implemented using the DIMES SIC3A IC process of Delft University of Technology. A chip photomicrograph is shown in Fig. 12.

In order to facilitate easy measurement of the system, all capacitors are off-chip.

As stated earlier, the wavelet transform allows analysis of the ECG signal focusing on the signal at various levels of detail. Analyzing the structure of the electrogram over multiple scales allows discrimination of electrogram signal features pertaining over all scales from those only seen at fine or coarse scales. Fig. 13 shows the measured response for 3 scales of the wavelet filter bank for the built-in (external) ECG signal of an Agilent 33120A signal

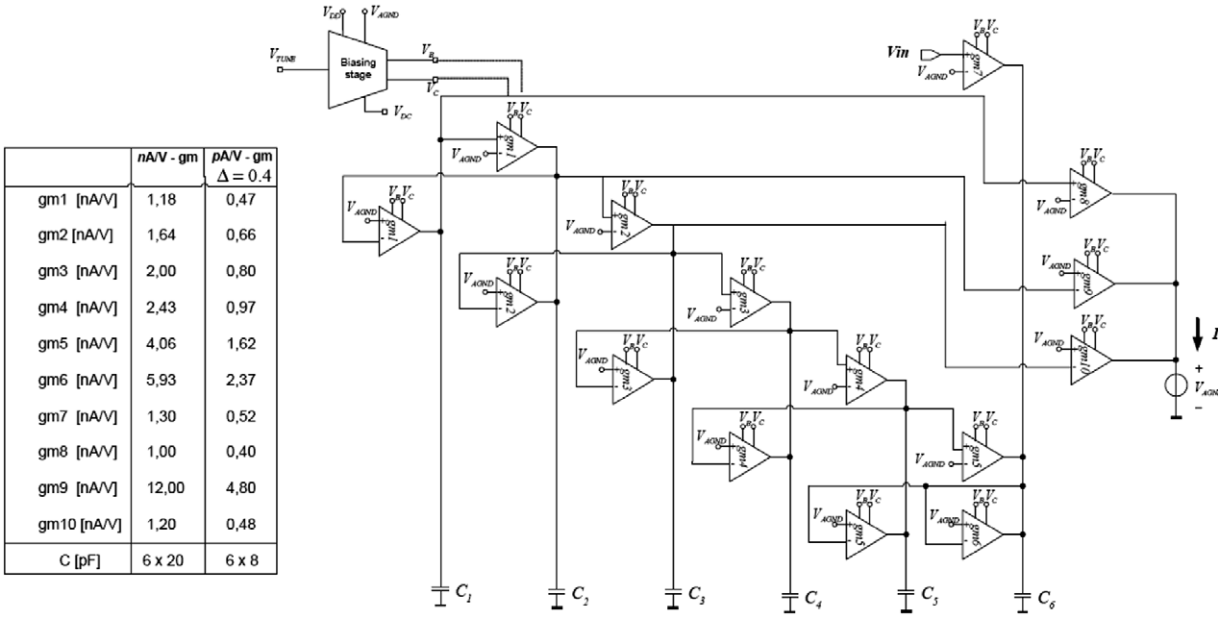

	nA/V - gm	pA/V - gm Δ = 0.4
gm1 [nA/V]	1,18	0,47
gm2 [nA/V]	1,64	0,66
gm3 [nA/V]	2,00	0,80
gm4 [nA/V]	2,43	0,97
gm5 [nA/V]	4,06	1,62
gm6 [nA/V]	5,93	2,37
gm7 [nA/V]	1,30	0,52
gm8 [nA/V]	1,00	0,40
gm9 [nA/V]	12,00	4,80
gm10 [nA/V]	1,20	0,48
C [pF]	6 x 20	6 x 8

Fig. 10. Block diagram of the sixth-order orthonormal wavelet filter employing transconductance–capacitor integrators.

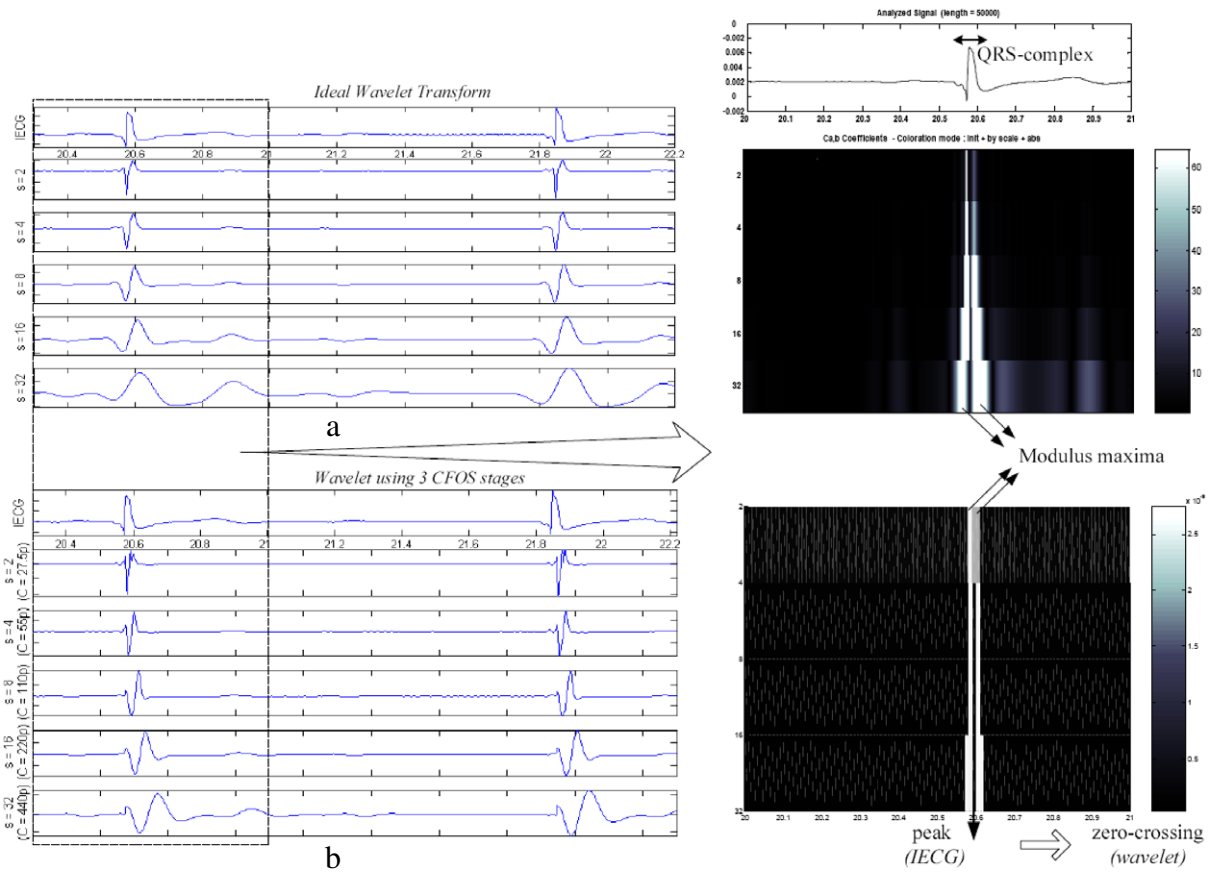

Fig. 11. (a) Ideal wavelet transform (5 scales), (b) sixth-order wavelet filter bank response (5 scales) for an intracardiac ECG input signal (left) and the detection of the modulus maxima (right).

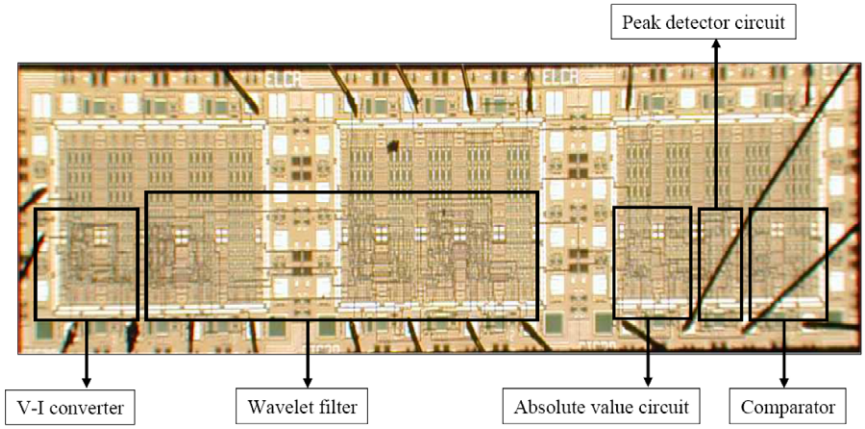

Fig. 12. Chip microphotograph of the QRS wavelet-based QRS modulus maxima detection system.

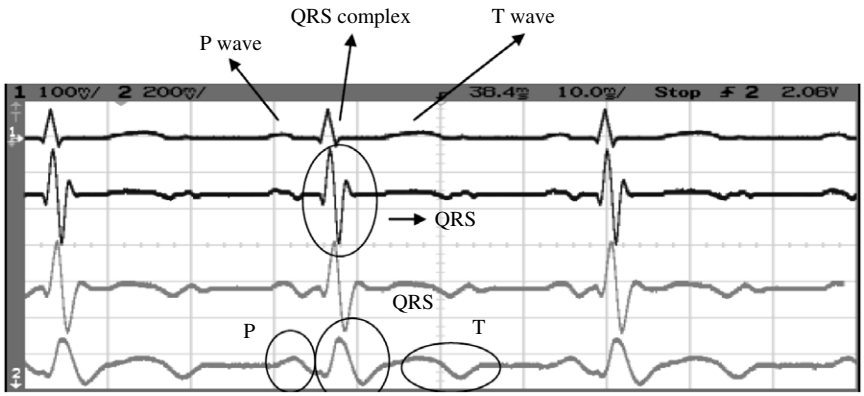

Fig. 13. Measured response of 3 scales of the system's wavelet filter bank (below) to a stylistic ECG signal (above).

generator. As one can observe from the figure, at very fine scales (smaller values of scale a), details of the electrogram, i.e., the QRS complex, are revealed. At coarse scales (larger values of a), the overall structure of the electrogram can be studied while overlooking at the details. Note that by this global view, the P-wave, the QRS complex and the T-wave can be more easily detected.

One of the important applications of wavelet transform is of in-band noise removal or denoising. The out-of-band noise can be removed by applying a linear time-invariant filtering approach like Fourier analysis based techniques. However, it cannot be removed when it overlaps the signal spectrum. Being a multiscale analysis technique, the wavelet transform offers the possibility of selective noise filtering and reliable parameter estimation. Denoising is based on correlation factor (amplitude) discrimination. This feature can be used to distinguish cardiac signal points from noise and interference, regardless of the frequency content of the noise. Fig. 14 displays a typical ventricular signal with additive white Gaussian noise (a random signal with a flat power spectral density), and the outputs of one wavelet filter ($a = 2^1$) and its subsequent absolute value detector. One can see that the wavelet filter can effectively remove the in-band and out-of-band noise present in the signal and the modulus maxima of the QRS complex are identified.

The total power consumption of the QRS wavelet-based QRS modulus maxima detector amounts to 550 nW (i.e., 110 nW per scale).

3.4.2. Ultra-wideband (UWB) communications using wavelets

Recently, the development of ultra-wideband (UWB) radio technology has been one of the most exciting progresses in the communications field. UWB radio technology not only promises enhanced data throughput with low-power consumption, but also provides high immunity against electromagnetic interference (EMI) and robust performance against to fading. It is expected that future short-range indoor UWB telecommunication systems will operate in the frequency band from 3.1–10.6 GHz according to the Federal Communications Commission (FCC). Although ultra-wideband communication offers significant resources and advantages its technological challenges also need to be addressed by researchers and communications engineers.

When implemented as impulse radio (IR–UWB) (i.e., where the information is transmitted by very short EM pulses) this new communication technology may revolutionize the way we think in wireless technology by modulating data in time rather than in frequency with

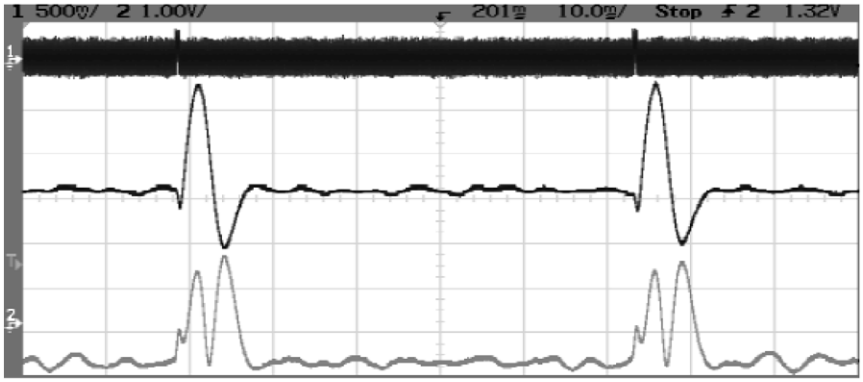

Fig. 14. Measured wavelet filter output (one scale, middle) and modulus maxima detection (bottom) when driven by a noisy ventricular IECG signal (top).

low-power consumption. From the perspective of traditional narrowband systems, the wideband nature of UWB systems requires a totally different design methodology of both the UWB front-end architecture and its constituting UWB circuit building blocks.

For IR–UWB, a convenient waveform to be transmitted is the Gaussian monocycle as it offers the best time–frequency resolution product. This feature is important for applications such as positioning and imaging. The Gaussian monocycle can be generated using a wavelet filter whose impulse response is the first derivative function of a Gaussian. For the filter topology, we can adopt the same topology as presented in the previous section or the one described in Ref. [41] comprising of a cascade of three complex first-order systems (CFOS) which in turn, consist of Gm-C sections employing differential pairs with partial positive feedback [42]. The entire impulse radio UWB transmitter is a combination of a pulse-position modulator (PPM) and a pulse generator (PG).

Fig. 15a shows the UWB transmitter IC mounted on its antenna printed circuit board (PCB). The antenna flares are the two Mickey-Mouse like ellipses on the back of the PCB and measures approximately 2 by 4 cm. The IC (see also the insert) is located in the middle of the PCB and measures 1.25 mm^2. The circuit has been designed using IBM 0.18 μm BiCMOS IC technology.

Fig. 15b displays the measured output waveforms of the pulse generator for transmitted "0" and "1" bits, respectively. A proper pulse position modulation is confirmed in the implementation.

Table 1 highlights the measured parameters of the impulse generator.

Table 1
Measured performance of the UWB transmitter.

Technology	0.18 μm BiCMOS (IBM)
Die area	1.25 mm^2
Active area	0.306 mm^2
Pulse width Gaussian monocycle	375 ns
PPM time delay	330 ns
Wavelet filter current consumption	14.4 mA at 1.8 V

4. Discrete-time signal processing applications of discrete wavelet (subband) transform

The effectiveness of wavelet (subband) transforms for discrete-time signal processing applications is due to their ability to provide efficient *sparse* representations for many natural signals. For example, sparse representations are important in coding. The image compression software on board NASA's Mars Rovers, designed for the requirements of deep-space communication, used wavelets; as does JPEG2K. Wavelet-based algorithms for noise reduction, deconvolution, interpolation, and dequantization, also rely on sparse representations. For some types of data, the wavelet transform does not provide a sparse representation; for these signals, other transforms or other non-transform based algorithms will be a better choice. Generically, the wavelet transform provides a sparse representation for piecewise smooth signals, like the scan-line of an image.

Many algorithms based on wavelet transforms have been proposed for the reduction of noise in signals and images. That is, the estimation of x from a noisy observation, $y = x + noise$. The most basic approach is to first compute the wavelet transform of the noisy signal, then to process the wavelet coefficient in an appropriate manner, generally, by reducing or *shrinking* in absolute value the small coefficients, and to lastly compute the inverse wavelet transform. The various algorithms differ in the way the wavelet coefficients are modified and in the type of wavelet transform utilized. Simple shrinkage rules include the soft-threshold and hard-threshold non-linearities. Denoising by wavelet-domain soft-thresholding can be written as

$$\hat{x} = W^{-1} S_T(Wy) \tag{30}$$

where W represents the wavelet transform, and W^{-1} represents the inverse wavelet transform, and where $S_T(v)$ represents the soft-threshold function with threshold T applied point-wise to the elements of the vector v. Improved denoising performance can be obtained when the thresholds are individually selected for each subband.

One class of algorithms for modifying the wavelet coefficients starts with some statistical model for the distribution of noise-free wavelet coefficients and uses Bayesian estimation theory to derive non-linear estimation procedures, a representative example being [43]. The soft-threshold denoising rule can also be derived in this way as the solution to a simple estimation problem. Many algorithms are obtained by postulating different prior

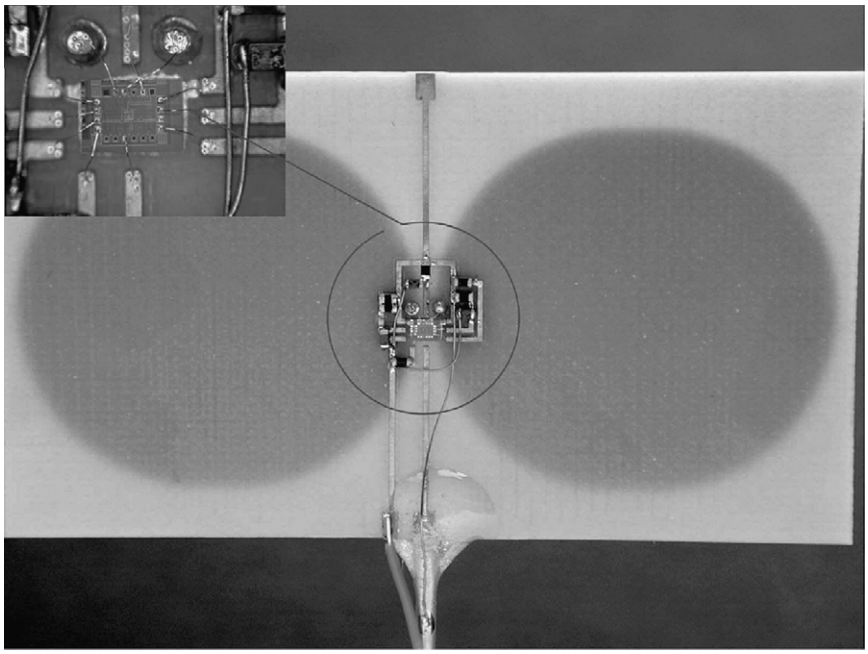

Fig. 15a. Integrated UWB transmitter mounted on the back side of the antenna.

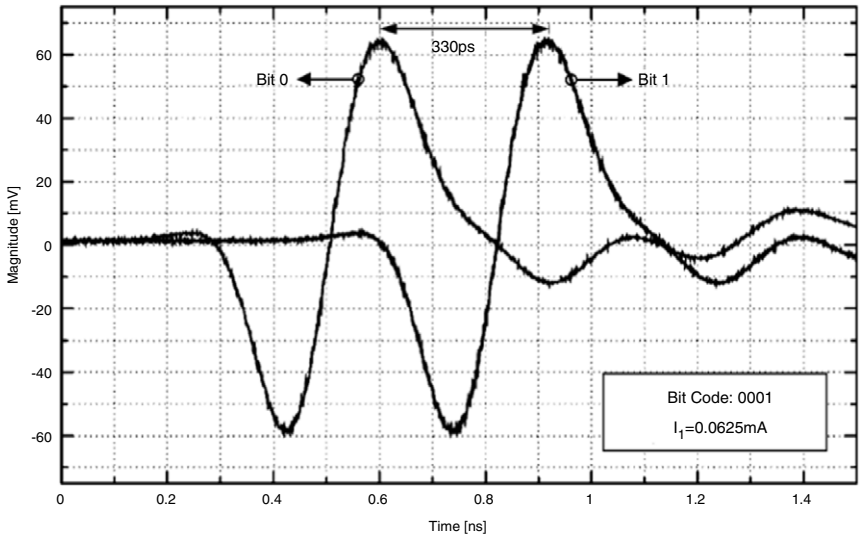

Fig. 15b. Measured pulse generator output waveforms while transmitting "0" or "1" bits.

distributions and various models to capture inter-scale and intra-scale dependencies. Another class of algorithms avoids the use of an explicit prior distribution. For example, the use of Stein's unbiased risk estimator, SURE, is proposed in [44] to determine an appropriate threshold for the soft-threshold rule. More recently, the SURE technique is used in [44,45] to create a computationally simple yet effective denoising algorithm in which optimal parameters of a parameterized non-linearity are obtained by minimizing SURE. For the non-linearities proposed in [44,45] the minimization requires only the solution to a small set of linear equations. To further improve performance, some denoising algorithms combine wavelet-coefficient thresholding with other criteria like total variation [46]. While most of the proposed wavelet-based denoising algorithms are developed for the case of additive independent white Gaussian noise, several methods have been proposed for the more difficult case of signal-dependent noise, e.g., Poisson, etc., which is important due to its relevance in medical imaging.

The restoration of degraded signals and images often requires correcting for blurring as well as reducing noise. Therefore, wavelet-based algorithms for combined deconvolution and denoising have also been developed which, like denoising algorithms, are motivated by the ability of wavelet transforms to provide sparse representations of

signals and images. Wavelet-based deconvolution algorithms are usually iterative. For the deconvolution problem, the observed data, y, is given by $y = Hx + noise$ where H is a known blurring operator and x is the unknown signal to be estimated. It turns out that a simple deconvolution algorithm can be derived which generalizes the soft-threshold rule. Specifically, the *Thresholded-Landweber* iteration is

$$w(k+1) = S_{(\lambda/2\alpha)}[w(k) + (1/\alpha)WH^T(y - HW^{-1}w(k))] \quad (31)$$

where $w(k)$ is the vector of wavelet coefficients at iteration k. The estimated signal is then given by $\hat{x} = W^{-1}w$. The *Thresholded-Landweber* iteration can be derived via estimation theory [47] or as the optimal solution to a deterministic functional [48]. In particular, the iteration in Eq. (31) minimizes the cost function

$$E = \left\|y - HW^{-1}w\right\|_2^2 + \lambda \|w\|_1 \quad (32)$$

where the first term measures the agreement with the observed data and the second term promotes wavelet-domain sparsity. The parameter λ controls how smooth the result is. λ is equivalent to the SNR in a Bayesian derivation of Eq. (31). The term α in Eq. (31) controls the rate of convergence of the iteration; small values of α increase the rate of convergence. But to ensure convergence to the optimal solution of Eq. (32) α should be greater than the maximum eigenvalue of $H^{-1}H$. Note that when H is the identity matrix (no blurring is present) and W is orthonormal, then the result obtained by the *Thresholded-Landweber* iteration is exactly the same as the result of applying the wavelet-domain *soft-threshold* rule. We note that the iteration in Eq. (31) is not the only way to minimize Eq. (32). Indeed, techniques have been developed to significantly speed up the convergence rate at least in some cases. The cost function in Eq. (32) is attractive in part because it is convex—the unique global minimizer can always be found. However, as in the case of denoising, by varying the cost function, or equivalently, by varying the prior distribution for w, various deconvolution algorithms can be obtained, potentially providing better results. To further promote sparsity the L_1-norm in Eq. (32) can be replaced by the L_0-norm which is non-convex. It is then much more difficult to obtain the exact optimal solution. However, approximate solutions to the L_0-norm criterion can be superior to the true L_0-norm criterion solution, depending on the problem.

A comparison between the L_0-norm and L_1-norm for several applications suggests that, for most natural images, the L_0-norm is the more effective of these two sparsity-promoting criteria [49]. One approach to obtain a representation approximately minimizing the L_0-norm is to perform iterative *hard-thresholding* with successively decreasing threshold values. In [49], it is shown that this approach can be formally derived using optimization principles. Examples in [49] illustrate excellent results for dequantization, super-resolution, and de-mosaicing.

For some classes of signals and images, no single transform can provide a sparse representation. Morphological Component Analysis (MCA) was developed for this case [50]. MCA uses two or more transforms together to obtain a sparse representation. There is no unique representation, so MCA asks for a representation that maximizes a total sparsity-promoting criterion. As a result, MCA can be used to solve the following separation problem. Suppose $s(t)$ is a superposition of two signals, $s(t) = s_1(t) + s_2(t)$. Also, suppose $s_1(t)$ is sparsely represented using transform F_1 and, likewise, $s_2(t)$ is sparsely represented using transform F_2. Then, provided the transforms of F_1 and F_2 are sufficient distinct, basis vectors of F_1 are roughly uncorrelated with basis vectors of F_2, then MCA can *approximately* recover $s_1(t)$ and $s_2(t)$. Examples in [50] illustrate how the shape and texture of an image can be separated using the curvelet transform and discrete cosine transform. One way to implement the MCA algorithm is by iterative thresholding, where the threshold is initialized with a large value and gradually reduced. The separation of a signal into components, blind source separation (BSS), is also the goal of Independent Component Analysis (ICA) which uses multiple observation signals. For certain signals, MCA can do that separation with a single observation signal. MCA algorithms have also been developed for the case where multiple observation signals is available, to provide a new approach to BSS.

The development and popularity of algorithms for wavelet-based discrete-time signal processing has led to the widespread appreciation of the power of sparse representations. In turn, this has led to the development of innovative new algorithms based on sparse representations that are not at all limited to wavelet-based signal processing.

5. Future research directions and conclusions

Historically speaking, analysis/synthesis filter bank configuration, also interchangeably called subband or wavelet transform, based digital image and video processing has been of great interest in the field due to its desirable multiresolution representation features for visual signals. Therefore, subband coding has become the main driver for early research activities on the subject widely reported in the literature. Similarly, synthesis/analysis filter bank configuration, so-called transmultiplexer, provides a theoretical framework to analyze and design popular multicarrier modulation techniques spanning from orthogonal frequency division multiplexing (OFDM) to code division multiple access (CDMA) communications techniques. More recently, wavelet transform with its sparsity (multirate) and flexible spectral properties has been effectively used for a variety of discrete-time signal processing applications including noise reduction or denoising, deconvolution, interpolation, and dequantization. We expect to see further studies in those interesting application areas in the future.

Although wavelet transform is defined in continuous time, its most popular applications reported in the literature have been in discrete-time domain. We emphasize on the built-in wavelet approximation errors in discrete-time processing as well as emerging and much less known analog applications of wavelet transform in this paper. A case in point, the wavelet transform is extremely versatile for the analysis of various electrophysiological signals (ExG)

like Electroencephalogram (EEG), Electromyogram (EMG), and Electrocardiogram (ECG). For example, neurological EEG signals represent rhythmic potential fluctuations on the head surface created by the synchronous discharge of nerve cells and has been used to diagnose epilepsy. One of the early signs of a seizure is the presence of characteristic transient waveforms in the EEG (spikes and sharp waves). The shape and size of these waveforms may substantially vary from one patient to another. The wavelet transform has been used as a detection tool due to the very mixed nature of these phenomena, and wavelet analysis was shown to be useful in identifying the localized features in the EEG signal. Therefore, one could apply the proposed low-power wavelet filter design methodology for EEG characterization in closed-loop implantable neurostimulator devices and cochlear implants.

We also expect new applications of two-dimensional wavelets for biomedical imaging in ultra-low-power environments, for instance artificial retinae. Wavelets have recently been applied to medical image compression and found to be very effective. However, power consumption is an important issue in a battery-operated artificial retinae design. Image computations usually require large arrays of pixels. Therefore, due to the required massive parallel processing for artificial implantable vision systems including large number of A/D converters (one A/D converter per pixel) it turns out to be impracticable. Hence, an analog implementation is feasible and much more efficient than a digital one with respect to power consumption and chip area metrics of a design.

More recently, the idea of using wavelets in the real-time sensing of radio spectrum for cognitive radio application has been forwarded [22]. We expect more research and development in communications field exploring potential use of wavelets in next generation technologies.

In conclusion, wavelet transform framework is a very elegant mathematical tool to design compactly supported orthogonal and bi-orthogonal continuous-time function sets or analog filter banks. It is expected to see an increased amount of research and technology development work in the coming years employing wavelets for various engineering applications.

Acknowledgments

The authors would like to acknowledge many invaluable contributions of Sumit Bagga, Sandro Haddad, Joel Karel, Ralf Peeters, Daniel Rocha, Arie van Staveren and Ronald Westra to this work; IBM Microelectronics for fabrication access and fabrication of the testchip, and the financial support for parts of this work by STW, the Dutch Technology Foundation.

References

[1] P.J. Burt, E.H. Adelson, The Laplacian pyramid as a compact image code, IEEE Trans. Communications (April) (1982) 532–540.
[2] M.J.T. Smith, T.P. Barnwell III, A procedure for designing exact reconstruction filter banks for tree-structured sub-band coders, in: Proc. IEEE ICASSP, 1984, pp. 27.1.1–27.1.4.
[3] F. Mintzer, Filters for distortion-free two-band multirate filter banks, IEEE Trans. ASSP (June) (1985) 626–630.
[4] P.P. Vaidyanathan, Quadrature mirror filter banks, M-band extensions and perfect reconstruction techniques, IEEE Signal Process. Mag. (July) (1987) 4–20.
[5] S. Mallat, Multiresolution Representations and Wavelets. Ph.D. Thesis, University of Pennsylvania, 1988.
[6] I. Daubechies, Orthonormal bases of compactly supported wavelets, Comm. Pure Appl. Math. (November) (1988) 909–996.
[7] P. Goupillaud, A. Grossmann, J. Morlet, Cycle-octave and related transforms in seismic signal analysis, Geoexploration (1984) 85–102.
[8] A. Grossmann, J. Morlet, Decomposition of Hardy functions into square integrable wavelets of constant shape, SIAM J. Math. Anal. (July) (1984).
[9] J.M. Combes et al. (Eds.) Wavelets: Time–frequency methods and phase space, in: Proceedings of the International Conference, Marseille, France, Dec. 1987.
[10] First NJIT Symposium on Multiresolution Decomposition Techniques: Wavelets, Subbands and Transforms, April 1990. http://web.njit.edu/ali/s1.htm.
[11] NSF/CBMS Conference on Wavelets, Univ. of Lowell, June 1990.
[12] A.N. Akansu, R.A. Haddad, H. Caglar, Perfect reconstruction binomial QMF-wavelet transform, SPIE Visual Comm. Image Process. (October) (1990) 360–367.
[13] I. Daubechies, Ten Lectures on Wavelets, SIAM, 1992.
[14] A.N. Akansu, R.A. Haddad, Multiresolution Signal Decomposition: Transforms, Subbands, and Wavelets, 1st ed., Academic Press, 1992.
[15] C.K. Chui, An Introduction to Wavelets, Academic Press, 1992.
[16] IEEE Signal Process. Mag. (March) (2008).
[17] S.A.P. Haddad, S. Bagga, W.A. Serdijn, Log-domain wavelet bases, IEEE Trans. Circuits Syst. - I 52 (10) (2005) 2023–2032.
[18] R.L.M. Peeters, J.M.H. Karel, R.L. Westra, S.A.P. Haddad, W.A. Serdijn, Multiwavelet design for cardiac signal processing, in: 28th Annual International Conference of the IEEE Engineering in Medicine and Biology Society, EMBC 2006, New York, Aug. 2006.
[19] J.M.H. Karel, R.L.M. Peeters, R.L. Westra, S.A.P. Haddad, W.A. Serdijn, An L2-based approach for wavelet approximation, in: Proc. CDC-ECC, Seville, Spain, Dec. 2005, pp. 7882–7887.
[20] D.A. Johns, W.M. Snelgrove, A.S. Sedra, Orthonormal ladder filters, IEEE Trans. Circuits Syst. 36 (3) (1989) 337–343.
[21] S. Bagga, A.V. Vorobyov, S.A.P. Haddad, A.G. Yarovoy, W.A. Serdijn, J.R. Long, Co-design of an impulse generator and miniaturized antennas for IR–UWB, IEEE Trans. Microwave Theory Tech. 54 (4) (2006) 1656–1666. (special Issue on UWB).
[22] Y. Hur, J. Park, W. Woo, K. Lim, C.-H. Lee, H.S. Kim, J. Laskar, A wideband analog multi-resolution spectrum sensing (MRSS) technique for cognitive radio (CR) systems, in: Proc. IEEE International Symposium on Circuits and Systems, May 2006, pp. 4090–4093.
[23] S. Bagga, S.A.P. Haddad, W.A. Serdijn, J.R. Long, Ultra-wideband radio: Unconventional circuit solutions for unconventional communication, in: Arthur H.M. van Roermund, Herman Casier, Michiel Steyaert (Eds.), Analog Circuit Design, Kluwer Academic Publishers, 2006.
[24] G.A. Baker Jr., Essentials of Padé Approximants, Academic Press, 1975.
[25] J.M.H. Karel, R.L.M. Peeters, R.L. Westra, S.A.P. Haddad, W.A. Serdijn, Wavelet approximation for implementation in dynamic translinear circuits, in: Proc. IFAC World Congress, Prague, Czech Republic, July 2005.
[26] L. Thiele, On the sensitivity of linear state–space systems, IEEE Trans. Circuits Syst. 33 (5) (1986) 502–510.
[27] M. Snelgrove, A.S. Sedra, Synthesis and analysis of state–space active filters using intermediate transfer function, IEEE Trans. Circuits Syst. 33 (3) (1986) 287–301.
[28] D.P.W.M. Rocha, Optimal Design of analogue low-power systems, A strongly directional hearing-aid adapter, Ph.D. Thesis, Delft University of Technology, April 2003.
[29] G. Groenewold, Optimal dynamic range integrators, IEEE Trans. Circuits Syst. I 39 (8) (1992) 614–627.
[30] K.S. Tan, P.R. Gray, Fully-integrated analog filters using bipolar-JFET technology, IEEE J. Solid-State Circuits 13 (6) (1978) 814–821.
[31] K.W. Moulding, G.A. Wilson, A fully-integrated five-gyrator filter at video frequencies, IEEE J. Solid-State Circuits 13 (3) (1978) 303–307.
[32] Y. Tsividis, Externally linear, time-invariant systems and their application to companding signal processing, IEEE Trans. Circuits Syst. II 44 (2) (1997) 65–85.
[33] J. Mulder, W.A. Serdijn, A.C. van derWoerd, A.H.M. van Roermond, Dynamic Translinear and Log Domain Circuits: Analysis and Synthesis, Kluwer Academic Publishers, Boston, 1999.
[34] R.W. Adams, Filtering in the log domain, in: Proc. 63rd Convention A.E.S., May 1979, pp. 1470–1476.

[35] E. Seevinck, Companding current-mode integrator: A new circuit principle for continuous-time monolithic filters, Electron. Lett. 26 (24) (1990) 2046–2047.
[36] D.R. Frey, Log-domain filtering: An approach to current-mode filtering, Proc. Inst. Elect. Eng., Pt. G 140 (6) (1993) 406–416.
[37] D.R. Frey, Exponential state space filters: A generic current mode design strategy, IEEE Trans. Circuits Syst. I 43 (1) (1996) 34–42.
[38] C. Toumazou, J.B. Hughes, N.C. Battersby (Eds.), Switched Currents: An Analogue Technique for Digital Technology, Peter Peregrinus, London, 1993.
[39] F.A. Farag, C. Galup-Montoro, M.C. Schneider, Digitally programmable switched-current FIR filter for low-voltage applications, IEEE J. Solid-State Circuits 35 (4) (2000) 637–641.
[40] L.C.C. Marques, W.A. Serdijn, C. Galup-Montoro, M.C. Schneider, A switched-MOSFET programmable low-voltage filter, in: Proc. SBMicro/SBCCI, Brazil, Sept. 2002.
[41] S.A.P. Haddad, R.P.M. Houben, W.A. Serdijn, Analog wavelet transform employing dynamic translinear circuits for cardiac signal characterization, in: Proc. IEEE ISCAS, vol. 1, Bangkok, Thailand, May, 2003 pp. 121–124.
[42] S. Bagga, A.V. Vorobyov, S.A.P. Haddad, W.A. Serdijn, A.G. Yarovoy, J.R. Long, Codesign of an impulse generator and miniaturized antennas for IR–UWB, IEEE Trans. Microw. Theory Tech. 54 (4) (2006) 1656–1666. Part 2.
[43] D.L. Donoho, I.M. Johnstone, Adapting to unknown smoothness via wavelet shrinkage, J. Amer. Statist. Assoc. 90 (432) (1995) 1200–1224.
[44] F. Luisier, T. Blu, M. Unser, A new SURE approach to image denoising: Interscale orthonormal wavelet thresholding, IEEE Trans. Image Process. 16 (3) (2007) 593–606.
[45] M. Raphan, E.P. Simoncelli, Optimal denoising in redundant representations, IEEE Trans. Image Process. 17 (8) (2008) 1342–1352.
[46] S. Durand, J. Froment, Reconstruction of wavelet coefficients using total variation minimization, SIAM J. Sci. Comput. 24 (5) (2003) 1754–1767.
[47] M.A.T. Figueiredo, R.D. Nowak, An EM algorithm for wavelet-based image restoration, IEEE Trans. Image Process. 12 (8) (2003) 906–916.
[48] I. Daubechies, M. Defrise, C. De Mol, An iterative thresholding algorithm for linear inverse problems with a sparsity constraint, Comm. Pure Appl. Math. 57 (11) (2004) 1413–1457.
[49] J. Portilla, L. Mancera, L_0-based sparse approximation: Two alternative methods and some applications, wavelet applications in signal and image processing X, in : Proc. SPIE 5207, San Diego, Aug. 2003.
[50] J.-L. Starck, M. Elad, D. Donoho, Image decomposition via the combination of sparse representation and a variational approach, IEEE Trans. Image Process. 14 (10) (2005) 1570–1582.

Ali N. Akansu received the B.S. degree from the Technical University of Istanbul, Turkey, M.S. and Ph.D degrees from the Polytechnic University, Brooklyn, New York, all in Electrical Engineering. Since 1987, he has been the faculty of the Department of Electrical and Computer Engineering at the New Jersey Institute of Technology. He was a Founding Director of the New Jersey Center for Multimedia Research and NSF Industry-University Cooperative Research Center for Digital Video. Currently, he is a Visiting Professor at the Courant Institute of Mathematical Sciences of the New York University performing research on Quantitative Finance.

Akansu was the Vice President for Research and Development of IDT Corporation. He was the founding President and CEO of PixWave, Inc., and Senior VP for Technology Development of TV.TV (IDT subsidiaries). He has been sitting on the boards of several companies and an investment fund. He was an academic visitor at IBM T.J. Watson Research Center and at GEC-Marconi Electronic Systems Corp. Dr. Akansu has published numerous articles and several books on his research work over the last two decades. His current research interests include signal and transform theories, and applications in finance, next generation Internet, wireless OFDM/CDMA communications and RF engineering. Dr. Akansu is a Fellow of the IEEE.

Wouter A. Serdijn received the M.Sc. (cum laude) and Ph.D. degrees from Delft University of Technology, Delft, The Netherlands, in 1989 and 1994, respectively. His research interests include low-voltage, ultra-low-power and ultra-wideband analog integrated circuits for wireless communications, pacemakers, cochlear implants, portable, wearable, implantable and injectable ExG recorders and neurostimulators. In this field, he is the co-editor and co-author of 7 books, 6 book chapters and more than 200 publications and presentations. He teaches Analog Electronics, Analog Signal Processing, Micropower Analog IC Design and Electronic Design Techniques. He received the Electrical Engineering Best Teacher Award in 2001 and 2004.

Serdijn has served as an Associate Editor for the IEEE Transactions on Circuits and Systems, both parts I and II, from 2002 to 2007, as chair of the Analog Signal Processing Technical Committee of the IEEE Circuits and Systems society, as technical program committee member of ISCAS, BioCAS, ICECS, BioDEVICES, APCCAS and ICUWB and currently serves as a member of the Board of Governors (BoG) of the Circuits and Systems Society (2nd term) in various roles, as Deputy Editor in Chief for IEEE Transactions on Circuits and Systems—I and as Technical Program Chair for the 2010 IEEE International Symposium on Circuits and Systems. He is a Senior Member and a mentor of the IEEE.

Ivan W. Selesnick received the B.S, MEE, and Ph.D degrees in Electrical Engineering in 1990, 1991, and 1996, respectively, from Rice University, Houston, TX. In 1997, he was a visiting professor at the University of Erlangen-Nurnberg, Germany. He then joined the Department of Electrical and Computer Engineering, Polytechnic Institute of New York University (then Polytechnic University), where he is an associate Professor. His current research interests are in the area of digital signal and image processing, wavelet-based signal processing, and biomedical signal processing.

In 1991 he received a DARPA-NDSEG fellowship. In 1996 Dr. Selesnick's Ph.D. dissertation received the Budd Award for Best Engineering Thesis at Rice University and an award from the Rice-TMC chapter of Sigma Xi. He received the Alexander von Humboldt Award (1997) and the National Science Foundation Career award (1999). He has been a member of the IEEE SPTM Technical Committee, an associate editor of the IEEE Trans. on Image Processing, of IEEE Signal Processing Letters, and is currently an associate editor of IEEE Trans. on Signal Processing.